Analyst

Accepted Manuscript

ROYAL SOCIETY OF CHEMISTRY

www.rsc.org/analyst

Analyst

RSCPublishing

ARTICLE

The role of lipid droplets and adipocytes in cancer. Raman imaging of cell cultures: MCF10A, MCF7, MDA-MB-231 compared to adipocytes in cancerous human breast tissue

Cite this: DOI: 10.1039/xoxxoooooox

Received ooth January 2012,
Accepted ooth January 2012

DOI: 10.1039/xoxxoooooox

www.rsc.org/

Halina Abramczyk,[a,*] Jakub Surmacki,[a] Monika Kopeć,[a] Alicja Klaudia Olejnik,[a] Katarzyna Lubecka-Pietruszewska[b] and Krystyna Fabianowska-Majewska[b]

We studied live nonmalignant (MCF10A), mildly malignant (MCF7) and malignant (MDA-MB-231) breast cancer cells and human breast cancer tissue. We demonstrate the first application of Raman imaging and spectroscopy in diagnosing the role of lipid droplets in cell line cultures that closely mimic an *in vivo* environment of various stages the human breast cancer tissue. We analyzed the composition of the lipid droplets in nonmalignant and malignant human breast epithelial cell lines and discuss the potential of lipid droplets as a prognostic marker in breast cancer. To identify any difference between the lipid droplet-associated biochemistry and to correlate it with different stages of breast cancer, the PCA method was employed. The chemical composition of lipids and proteins, both in the cell line models and in the human breast tissue has been analyzed. The paper shows the alterations in lipid metabolism that have been reported in cancer, at both cellular and tissue levels, and discuss how they contribute to different aspects of tumourigenesis.

Introduction

Vibrational imaging reveal new expanses in cancer biology. In the last decade, confocal Raman microspectroscopy has been proved to be a promising contactless and nondestructive method suitable for determination of intracellular chemical composition and chemical imaging of living cells, and human tissues that may be used to diagnose a variety of diseases. Vibrational spectroscopy may someday replace standard but unsatisfying medical procedures. One of the main advantages of Raman imaging is that it can give spatial information about various chemical constituents in defined cellular compartments in contrast to methods (e.g. liquid chromatography- mass spectrometry (LC-MS)) that must rely on bulk or fractionated analyses of extracted components.

Raman and IR imaging combined with nonlinear laser spectroscopy have brought revolution in cancer detection and treatment.[1-3] High spatial and temporal resolution of these methods allows to detect a single cancerous cell in vivo and monitor molecular events that may contribute to cancer development. The recent results obtained by Raman imaging and femtosecond transient absorption demonstrate that there are many signaling pathways and metabolic alterations responsible for tumorigenesis.

The link between cancer and the altered metabolism is usually described through the mechanism of glycolysis, known as the Warburg effect, which replaces ATP generation through oxidative phosphorylation by ATP generation through glycolysis, even under normal oxygen concentrations.[4]

There is more and more evidence[1,3,5-9] that metabolic alterations in tumors extends beyond the Warburg effect and other pathways are equally important, particularly those associated with lipoprotein metabolism and the production of fatty acids activated via multiple lipogenic enzymes affected at all levels of regulation, including transcription, translation, protein stabilization and protein phosphorylation.[10-12] The recent reviews[13] emphasize the role of lipid synthesis in cancer metabolism and tumor development. Although fatty acid (FA) and cholesterol biosynthesis occur mainly in liver, adipose, and lactating breast tissues, lipid biosynthesis is also observed in cancerous tissue that is required for the rapid proliferation of cancer cells. It has been reported that the shift from lipid uptake

to *de novo* lipogenesis in cancer cells leads to increased membrane lipid saturation, resulting in higher levels of saturated and monounsaturated phospholipids, potentially protecting cancer cells from oxidative damage by reducing lipid peroxidation.[14]

Increased level of saturated FAs are found in aggressive breast cancers, suggesting that reduced membrane fluidity is a feature of the advanced disease.[10] Furthermore, depletion of sterol regulatory element-binding transcription factor 1 (SREBP1) and 2 (SREBP2) diminishes levels of monounsaturated FAs, resulting in mitochondrial dysfunction, the accumulation of reactive oxygen species (ROS) and endoplasmic reticulum (ER) stress in immortalised human epithelial cells.[15]

The lipid phenotype was ignored for many years by the Raman scientific community that has focused almost exclusively on the proteome profile in Raman and IR spectra.[16-19]

As a consequence of focusing on the role of the proteome profile in tumorigenesis, the optical methods, including Raman spectroscopy, monitored the main organelles that are important in making proteins: nucleus, ribosomes, rough endoplasmic reticulum and Golgi apparatus. Lipid droplets were mostly ignored in this respect and regarded mainly as static energy storage deposits. However, recent research gained new exciting perspectives for lipid droplets showing that they represent important organelles containing specialized proteins and lipids which play essential roles in cell signaling, regulation of lipid metabolism, membrane trafficking and control of the synthesis and secretion of inflammatory mediators.[20-21]

Lipid droplets typically consist of neutral lipids in the form of triacylglycerols, cholesteryl esters, or retinyl esters surrounded by a phospholipid monolayer and proteins at the surface of lipid droplets. In addition to storing triglycerides for energy, lipid droplets also store phospholipids and sterols, which are critical for the growth and maintenance of the cell membrane.[22] Lipid droplets have important roles in cellular lipid homeostasis and energy metabolism. They have also major significance in the development of metabolic and infectious diseases: atherosclerosis, lipodystrophy and insulin resistance, Chanarin-Dorfman syndrome, and liver damage.[23] The recent research showed that they also have significant roles in many aspects of cancer development.[23-29]

In view of these fundamental discoveries, lipid droplets are under intensive study due to the increasing recognition that they have fundamental roles in cellular metabolism. Lipid metabolism is an emerging field in cancer research and there is increasing evidence that lipid biomarkers should be considered a crucial hallmark of cancer.[3,6,12,27] However, the functional implications of lipid droplets are poorly understood. Cancer cells seem to contain increased numbers of lipid droplets compared with normal cells. This was observed in colon adenocarcinomas[27] as well as in a human lung cancer cell (A549).[30] Contrary, some papers suggest that cancer suppresses the formation of lipid droplets and decreases the corresponding lipid pool.[31-33] In contrast to the results obtained for cell cultures, recent Raman[1,3,6] and nuclear magnetic resonance studies have shown that the concentration of lipids in breast cancer tissue is significantly lower compared to healthy tissue.[34,35]

The reason of this apparent discrepancy is unknown, although it has been suggested[1,3,6] that an increase of intracellular lipids in healthy tissue may origin from extracellular matrix, which does not exist in cell cultures. This signature of cancer in the human tissue is particularly important for invasive ductal and lobular breast cancers when the epithelial cells migrate and invade through the basement membrane into the surrounding extracellular matrix consisting of connective tissue, fibroblasts and adipose tissue that is a reservoir of lipids.[1,3,6] We have demonstrated by Raman imaging that the noncancerous breast tissue contains a markedly higher concentration of lipids than the cancerous tissue from the tumor mass.[3,6] This conclusion is consistent with reports that women with dense breasts are more likely to be diagnosed with breast cancer and the breast cancer is likely to be more aggressive. Dense breasts have less fatty tissue and more non-fatty tissue. Breasts that aren't dense have less non-fatty tissue and more fatty tissue contains adipocytes.[36] Unlike most cell types, white adipocytes typically contain a single, large lipid droplet ranging up to 100 μm in diameter that occupy the majority of the cytosol. In most other cell types, including the epithelial cells, multiple and small lipid droplets, usually of less than 1 μm in size are observed.[37] Although the functional implications of the vastly different sizes of lipid droplets are poorly understood it is obvious that the geometry is subject to different physical and chemical properties that may determine their various biological functions.

The major role of white adipocytes is related to storing energy supply. However, our recent results showed that they also serve as a reservoir of anti ROS species (particularly carotenoids) which may play a protective role against cancer by increasing the resistance of cells to oxidative stress.[2,3,6] The protective role of selected fatty acids, such as docosahexaenoic and eicosapentaenoic acids, have been observed in mammary tumor initiating cells[28,29] by reducing the proliferation of mammary tumor initiating cells and increasing toxicity towards. It has been suggested that the positive or negative effect of some n-3 or n-6 fatty acids may be due to alteration of the lipid profile with transformation to prostaglandins.[38] Thus, the protective character of some fatty acids may suggest that cancer cells should contain decreased numbers of lipid droplets compared with normal tissue. However, the protective role has been proved to the limited number of fatty acids[39] and the other fatty acids pose more potential toxicity to cells compared to neutral esterified triacylglycerides. Increased accumulation of lipid droplets seems to play a role in protection from lipotoxicity. Lipid droplets provide a protection mechanism to avoid apoptosis when cells are exposed to excess unesterified fatty acids.[40] In light of the diverse roles of lipids in membrane structure, cellular signaling and protein regulation, it is obvious that lipids are essential components of the cellular machinery that regulates proliferation, migration and survival of cancer cells. Recent technological advances, such as the accurate detection and quantitation of numerous lipid species by mass spectrometry, allow the profiling of discrete changes within the

lipid composition of cancer cells and will help to elucidate the intricate connections between lipid metabolism and cell function in cancer. Lipid droplets have also been extensively studied by vibrational spectroscopy.[41-44]

The goal of our study was to assess the impact of cancer aggressiveness on the amount of cytosolic lipid droplets in nonmalignant and malignant human breast epithelial cell lines. We will study live nonmalignant (MCF10A), mildly malignant (MCF7) and malignant (MDA-MB-231) breast cancer cells. This paper will examine some of the alterations in lipid metabolism in breast cancer by Raman imaging, and discuss how they contribute to different aspects of tumourigenesis in malignant human breast epithelial cell lines MCF7, MDA-MB-231 compared to nonmalignant MCF10A cell lines. The paper analyzes the composition of the lipid droplets in nonmalignant and malignant human breast epithelial cell lines and discuss the potential of lipid droplets as a prognostic marker in breast cancer.

Experimental

In order to employ Raman microspectroscopy for routine use in cell biology numerous technical and methodological problems need to be solved, such as discrimination of spectral contributions from cultivation media and supporting materials, adequate fixation assuring both viability and immobility of the cells during exposure to laser beam, compromise between high spatial resolution and inherent weakness of Raman signal, long acquisition times needed to improve signal-to-noise ratio, acquisition of Raman spectra and their preprocessing, as well as interpretation of complicated and overlapping pattern of Raman spectra in the terms of concentrations of chemical constituents.[45]

Cell lines and culture conditions

We studied live nonmalignant (MCF10A), mildly malignant (MCF7) and malignant (MDA-MB-231) breast cancer cells. MCF10A (tissue: mammary gland/breast, cell type: epithelial, CRL-10317) and MCF7 (tissue: mammary gland/breast; derived from metastatic site: pleural effusion, cell type: epithelial, HTB-22) were purchased at ATCC (American Type Culture Collection, LGC Standards). MDA-MB-231 (tissue: mammary gland/breast; derived from metastatic site: pleural effusion, cell type: epithelial, HTB-26) was purchased at ECCC (European Collection of Cell Cultures, Salisbury UK).

MCF10A cells were propagated in monolayer culture using standard mammalian cell culture techniques as described in the ATCC protocols. MCF10A cells were incubated at 37°C, at atmosphere of air, 95% humidity; carbon dioxide (CO_2), 5% in a nutrient-rich MEBM medium along with the additives obtained from Lonza/Clonetics Corporation as a kit: MEGM, Kit Catalog No. CC-3150 containing h-EGF-β (human epidermal growth factor), BPE (bovine pituitary extract), hydrocortisone and human recombinant insulin. According to the ATCC protocol we did not use the gentamycin-amphotericin B mix provided with kit. To make the complete growth medium, we added the 100 ng/ml cholera toxin from SIGMA (St. Louis, MO, USA) (sold separately).

MCF7 and MDA-MB-231 cells were cultured in EMEM medium (MEM Eagle with Earle's BSS, Lonza, Verviers, Belgium) and L15 medium (Leibovitz's L15 medium, Lonza), respectively, supplemented with: 2 mM L-glutamine; 0.01 mg/ml bovine insulin (only for MCF7 cells) (Sigma-Aldrich, St. Louis, MO, USA); 10% (and 15% for MDA-MB-231 cells) fetal bovine serum (FBS) (Thermo Scientific, HyClone, heat inactivated); 1 U/ml penicillin, and 1 μg/ml streptomycin (Life Technologies, Scotland, UK). Cells were grown at 37°C in a humidified atmosphere of 5% CO_2, except for MDA-MB-231 cells incubated without CO_2.

Cells were subcultured every 3–4 days after reaching 70–80% confluency. Cells were trypsinized, centrifuged, and resuspended in medium at a suitable density.

For the experiments, MCF10A, MCF7 and MDA-MB-231 cells were seeded onto calcium fluoride windows (CaF_2, 25×2 mm) at a low density of 10×10^3, 22×10^3 and 16×10^3 cells/cm^3, respectively. After 24 h the CaF_2 slides with cells were rinsed with phosphate-buffered saline (PBS, SIGMA P-5368, pH 7.4 at 25°C, c= 0.01 M) to remove any residual medium and confocal Raman measurements were made immediately. Cells were stored in PBS during measurements no longer than 1.5 hour.

For histological determination of lipid droplets in the cells we used the procedure from ref.[46] The samples were washed with PBS, fixed in 4% buffered formaldehyde at 4°C for 30 minutes and washed once with distilled water, then stained with Oil-Red-O (O0625 Sigma-Aldrich; saturated solution in isopropanol, diluted 3:2 in distilled water; EMD Millipore). Slides were photographed under a Olympus BX51 microscope (Olympus Corporation).

All procedures were conducted under a protocol approved by the institutional Bioethical Committee at the Medical University of Lodz, Poland (RNN/45/14/KE).

Raman microspectroscopy and imaging

To explore morphological and biochemical heterogeneity within cells Raman images were acquired using a confocal Raman microscope - WITec alpha 300 RSA (Ulm, Germany) consisting of an Olympus microscope, coupled via the fiber of a 50 μm core diameter with a 300 mm Czerny-Turner monochromator (Princeton Instruments Acton SP23000-300 mm Imaging Triple Grating Monochromator/Spectrograph) and a thermoelectrically cooled CCD camera ANDOR Newton DU970N-UVB-353 (EMCCD chip with 1600x200 pixel format, 16 μm dimension each) operating in standard mode at -64°C with full vertical binning. To obtain well spatially-resolved Raman spectra restricted to the lipid droplet volume, the 40x objective (NIKON CFI Plan Fluor C ELWD 40x: N.A. 0.60, W.D. 3.6-2.8 mm; DIC-M, C.C.0-2) was used in combination with small confocal pinhole (fiber core diameter 50 μm) to eliminate Raman signal from the CaF_2 slide. The laser beam doubled SHG of the Nd:YAG laser (532 nm) was focused on the sample with the objective to the laser spot of 1

μm determined by the laser wavelength and microscope objective being used. The average laser excitation power was 38 mW, the collection (integration) time of 0.5 s for Raman images and 20 s and 2 accumulations for single Raman spectra in the spectral ranges of 100-1780 cm^{-1} and 2600-3940 cm^{-1}. Rayleigh scattered light was removed using an edge filter. Under these experimental conditions, we did not observe any burning or photodegradation of the cells because PBS aqueous solution protects the sample. A piezoelectric table was used to record Raman images. Spectra were collected at one acquisition per pixel and a diffraction grating with 1200 lines/mm. Raman images (spatial resolution 1x1 μm) from the various spectral regions corresponding to the characteristic regions of proteins, fatty acids, DNA/RNA vibrations of the breast epithelial cells were constructed.

Data pre-processing and multivariate data analysis

An essential role in spectroscopic methods of molecular biology is played by preprocessing of Raman data, as they naturally occur at the expense of introducing some fixatives, matrices, adhesives, grow medium, which may generate their own vibrational spectra overlapping the signals from the native cells or tissue. To obtain reliable results one must be sure that the method of cell lines processing does not distort the vibrational spectra of the studied biological material. Detailed methodology is available elsewhere.[3]

Raman data collected with the CCD detector were pre-processed using the WITec Control/Project Plus 1.6/Project 2.10 package. The raw Raman data were corrected for cosmic rays. We used spatial and frequency filtering to remove sharp spikes attributed to cosmic rays.[47,48] The cosmic rays corrected data were smoothed (order:3, 7pt) by a Savitzky and Golay procedure.[49]

The raw Raman data were analyzed in the ranges of 100-1800 cm^{-1} and 1800-3940 cm^{-1}. The range of 100-1800 cm^{-1} is useful for control purpose, because it contains the band of the CaF_2 support at 321 cm^{-1}. The Rayleigh scattering and the Raman spectrum of the CaF_2 support were removed by background subtraction and reduction of the spectral range to 400-1800 cm^{-1} before multivariate analysis.

The Raman spectra were analyzed using the Principal Component Analysis (PCA) method and MATHLAB least-squares fitting algorithm using PLS_Toolbox Version 4.0 for use with MATLAB.[50] The large number of spectra collected for PCA analysis required the use of automated removal method for all of the spectra, which is critical to remove sources of variability arising from autofluorescence and substrate contamination. After baseline removal, the dominant remaining source of distinction between spectra is the intensity of the Raman features, arising from the variable amount of biological material within the sample. Finally, the spectra were normalized using the integral intensity of the band of water OH-stretching vibrations at 3400 cm^{-1} as an internal intensity standard.

Statistical evaluation of datasets and visualization of their spectral variability were based on the factor scores. The 2D array images of tens of thousands of individual Raman spectra were evaluated by the basis analysis method. In this method, each measured spectrum of the 2D spectral array is compared to basis spectra using a least squares fit. Such basis spectra are created as the average spectra from three characteristic areas in the sample. The weight factor at each point is represented as a 2D image of the corresponding color. The color code of Raman maps were based on the integrated Raman intensities in specific regions (sum option in the filter manager in the Witec project Plus 2.10). Using a lookup table, bright yellow colors indicate the highest intensities, whereas brown colors indicate the lowest intensities of the chosen region.

Results and discussion

Fig. 1 shows intracellular structures of MCF10A, MCF7 and MDA-MB-231 mapped by Raman microscopy. The comparison with the video images shows that Raman microscopy is capable of displaying the cell morphology. As shown in Fig. 1 the Raman and video images of the intracellular structures are of virtually identical shapes, revealing well-defined subcellular morphological structures. However, Raman can reveal not only morphological but also valuable information on detailed biochemical composition. The Raman images in the region of characteristic vibrations reveal well-defined protein structures, lipid droplets, membranes without need of staining. Thus, chemical composition of the intracellular structures can be furthermore analyzed in detail, although reliable spectral assignment and decomposition into the spectra of pure constituents should be carefully and critically evaluated.

Fig. 1 The video images and respective Raman images of MCF10A (A), MCF7 (B) and MDA-MB-231 (C) intracellular structures: lipid structure (triacylglycerides (TAGs), fatty acids (FA) and cholesterol esters (CEs) (2840-2900 cm^{-1}), lipid-protein structures (2900-3000 cm^{-1}) of live breast cells in PBS.

The protein and lipid structures are given with the proper spectral filters: lipid structure (triacylglycerides (TAGs), fatty acids (FA) and cholesterol esters (CEs) (2840-2900 cm^{-1}), lipid-protein structures (2900-3000 cm^{-1}).[1,3,6]

In this paper we will concentrate on lipid droplets. The lipid droplets are clearly seen in all types of cells presented in Fig. 1. In the Raman images they are represented by small bright spots, particularly clearly visible at the filters 2840-2900 cm^{-1} and 2900-3000 cm^{-1} typical for fatty acids, and triglycerides.[1,3,6] Histological staining with Oil-Red-O provided identical distribution of lipid droplets within the cells.

The size of the intracellular droplets vary in size, ranging from fractions of micrometers to a few micrometers.[52] Lipid droplets are typically localized in strings adjacent to the lysosome (Fig. 1B) or randomly distributed in the cytosol (Fig. 1C). They are also frequently observed inside the lysosome.

Fig. 2 shows the schematic cross section of an animal cell with the localization of lipid droplets.

Fig. 2 Cross section of an animal cell (A), video image of a single cell of MCF7 (B) and lipid droplet (C).

Fig. 3 shows Raman spectra across the marked lines inside the cells. Combining information contained in the chemical groups related to nucleic acids, proteins, and lipids,[3,53,54] which can be identified by appropriate peaks in the Raman spectra in Fig. 3, with the morphological structure recorded by both Raman and video images, the cellular components can be readily distinguished.

Fig. 3 Raman spectra across the marked lines inside the cells: MCF10A (A), MCF7 (B) and MDA-MB-231 (C). Spectra were normalized to the integral intensity of the water OH-stretching band at 3400 cm^{-1} as an intensity standard.

While it is difficult to perform the full vibrational analysis of the cell or the tissue due to heterogeneity of the sample and high spatial resolution of Raman microspectroscopy based on their single Raman spectra it is useful to identify first global changes in the structure and composition that are provided by the average Raman spectra.

Fig. 4 shows the average Raman spectra of MCF10A, MCF7 and MDA-MB-231.

Fig. 4 Average Raman spectra (A,C,E,G) and average difference Raman spectra (B,D,F,H); (A-D) model preprocessing: smoothing, baseline, Standard Normal Variate (SNV); (E-H) model preprocessing: smoothing, baseline, spectra are normalized to the integral intensity of the water OH-stretching band at 3400 cm^{-1} as an intensity standard; Cross-validated PLSDA Y-prediction plots for MCF10A (I), MCF7 (J), MDA-MB-231 (K).

The difference spectra of MCF7 and MDA-MB-231 to the controls MCF10A (Figs. 4B, 4D, 4F, 4H) suggest increased lipid content (positive peaks at 2844, 2859, 2906 cm^{-1}) and mixed proteome (negative peaks at 1630 cm^{-1} and positive peaks at 1004, 1270, 1662, 2962 cm^{-1}) in cell line of MCF7 and MDA-MB-231 compared to MCF10A. The enhanced lipid profile corresponds to increased numbers of lipid droplets in malignant and metastatic cells compared with non-malignant cells of MCF10A as the 2844, 2906 cm^{-1} peaks are typical of neutral esterified triacylglycerides that are the main components of the lipid droplet. The protein Amide I band at 1662 cm^{-1} shows increased proteome by strong positive spectral feature and is consistent with variation of Amide III at 1270 cm^{-1} and the protein band at 2962 cm^{-1}. The Raman bands at 835, 991, 1002, 1322, 1348 and 1630 cm^{-1} arise from the ring structures of tyrosine/phenylalanine/tryptophan, respectively.[55-61] The bands are more intense in cancer cells (Fig. 4D), suggesting possible elevation in the expression of such aromatic amino acids rich proteins. The protein bands at 835, 991, 1270, 1630, 1662, 2962 cm^{-1} show consistent variation with the protein band at 2930 cm^{-1}, which increases in MDA-MB-231 compared to non-malignant MCF10A and shows no change in MCF7. The band at 2930 cm^{-1} corresponds to collagen.[62,63] Although MCF10A is non-malignant cell line, it is characterized by collagen production due to fibrocystic disease of epithelium. This may explain the negligible difference between MCF10A and MCF7 Raman spectra (Fig. 4F).

To quantify the number of the lipid droplets in the three cell lines we have counted the droplets from the classical staining with Oil-Red-O and Raman images from the fixed regions of 120 μm x 120 μm. We have found that the number of cytoplasmic lipid droplets in live nonmalignant MCF10A breast cells is ≈4 times lower than in a highly malignant breast cells (MDA-MB-231) and ≈2 times lower than in a mildly malignant breast cells (MCF7). Thus, an increased amount of lipid droplets correlates with increased aggressiveness of cancer. The increased amount of cytoplasmic lipid droplets in the human breast cell may be closely related to increased rate of lipid synthesis in cancerous tissues.

The enhanced lipid content in malignant breast cancer cells may come from high rate synthesis of fatty acid and phospholipids.[64] This enhanced metabolism of transformed cells has long been recognized, because *de novo* synthesis provides the majority of lipids required for the rapid proliferation of cancer cells.[65] However, the detailed role of lipids in cellular transformation, tumour development and tumour progression, as well as their potential role in facilitating the spread of cancerous cells to secondary sites, are not yet fully understood.[13] The lipogenesis regulated by fatty acid synthase is associated with upregulation of HER1/HER2 tyrosine kinase receptors in the cells.[66,67] Our results indicate augmented lipogenic process as well as the excessive expression of tyrosine receptors observed in Fig. 4D, which might play an important role in promoting the upregulation of fatty acid synthase in both cancer cells of MCF7 and MDA-MB-231 compared to control epithelial cells of MCF10A.

So far we analyzed the average Raman spectra that provide information about the total cellular chemical content. Now, we will concentrate on the composition of the individual lipid droplets that amount to a marked increase in total cellular lipid content.

Fig. 5 shows the Raman images of the MCF10A, MCF7 and MDA-MB-231 cell that contain lipid droplets and the Raman spectra recorded at the middle of the lipid droplets (marked with the crosses).

Fig. 5 Video images, label-free Raman images (2840-2900 cm^{-1}) and Raman spectra from the characteristic structures (marked by the cross) of the lipid droplets in the live cells MCF10A (A), MCF7 (B) and MDA-MB-231 (C).

It is of interest to know whether chemical composition of the large adipocytes in human breast tissue is the same as that in the lipid droplets in the malignant and non-malignant epithelial cells.

Fig. 6 Comparison of the Raman spectra from the human adipose tissue (at the point marked with the green cross +) in the cancerous breast tissue (infiltrating ductal carcinoma, P104) and from the lipid droplets in the epithelial cells of MCF10A, MCF7 and MDA-MB-231.

Fig. 6 shows the comparison of the Raman spectra from the human adipose tissue (infiltrating ductal carcinoma), and from the lipid droplets in the epithelial cells of MCF10A, MCF7 and MDA-MB-231. It is evident that the lipid profiles of the non-adipocyte lipid droplets in epithelial breast cells differ markedly from that of the adipocyte indicating different chemical composition. The intracellular droplets in MCF10A, MCF7, MDA-MB-231 cells varies in size, ranging from a few micrometers to 10 μm (Figs. 6B, 6C, 6D). They are smaller than adipocytes of the human breast tissue. Adipocytes are lipid bodies that tend to be larger than lipid droplets ranging up from 30 to 100 μm (Fig. 6A).

These results demonstrates power of Raman imaging that can give spatial information about lipids in defined cellular compartments in contrast to liquid chromatography-mass spectrometry (LC-MS) that rely on bulk or fractionated analyses of extracted lipids.[42]

Different chemical composition suggests that the large adipocytes in the breast tissue play different role than the lipid droplets in the epithelial breast cells. To answer this fundamental question let us concentrate on the chemical composition of lipids in the breast adipocytes and in the lipid droplets.

Fig. 7 shows Raman spectra of selected omega 6 family fatty acids: linoleic acid (LA), γ-linolenic acid (GLA), arachidonic acid (AA) (A); oleic acid (OA), gliceryl trioleate, stearic acid, cholesterol, adipocyte from the cancerous breast tissue (infiltrating ductal carcinoma), lipid droplets from the nonmalignant and malignant epithelial cells: MCF10A, MCF7, MDA-MB-231, cancerous tissue (B and C); and selected omega 3 fatty acids: α-linolenic acid (ALA), eicosatetraenoic acid, eicosapentaenoic acid (EPA), docosapentaenoic acid (DPA), docosahexaenoic acid (DHA), tetracosapentaenoic acid, tetracosahexaenoic acid (D).

Fig. 7 Comparison of Raman spectra of adipocyte from the cancerous breast tissue (infiltrating ductal carcinoma) of patient 104 (adipocyte), lipid droplets from the nonmalignant and malignant epithelial cells: MCF10A, MCF7, MDA-MB-231 (B) with selected omega 6 family fatty acids: linoleic acid (LA), γ–linolenic acid (GLA), arachidonic acid (AA) (A); oleic acid (OA), gliceryl trioleate, stearic acid, cholesterol (C), and selected omega 3 fatty acids: α-linolenic acid (ALA), eicosatetraenoic acid, eicosapentaenoic acid (EPA), docosapentaenoic acid (DPA), docosahexaenoic acid (DHA), tetracosapentaenoic acid, tetracosahexaenoic acid (D).

Comparison of the Raman spectra of lipid bodies from the cells and the adipose of the breast tissue with the Raman spectra of saturated and unsaturated fatty acids and esterified fatty acids[3,60] presented in Fig. 7 shows that the adipocytes in the cancerous breast tissue (Fig. 7B) are dominated by triglycerides of oleic and linoleic acid. This is in agreement with the previous reports that approximately 60 to 85% of the weight of white adipose tissue is lipid, with 90-99% being triglyceride. Small amounts of free fatty acids (myristic, palmitic, palmitoleic, stearic, oleic and linoleic), diglyceride, cholesterol, phospholipid as well as cholesterol ester and monoglyceride are also present. The remaining weight of white adipose tissue is composed of water (5 to 30%) and protein (2 to 3%). Varying the composition of diet can vary the fatty acid profile in adipose tissue.[68]

By contrast, non-adipocyte lipid droplets (Fig. 7B) in the cancerous epithelial cells contain triglycerides and fatty acids dominated by arachidonic acid profile (Fig. 7A). It suggests that lipid droplet synthesis and growth is stimulated by different pathways compared to adipocytes. This important finding may indicate that the lipid droplets are potential bodies for localization of enzymes responsible for formation of eicosanoids. Our results are in agreement with the reports on lipid droplets abundantly present in leucocytes engaged in inflammation and cancer,[28,69] which are rich in estrified arachidonate. Eicosanoids are produced from arachidonic acid, a polyunsaturated 20-carbon FA. Arachidonic acid is converted into prostaglandin H_2 (PGH_2) by prostaglandin H_2 synthases, also known as cyclooxygenases (COX1 and COX2), or into leukotrienes by leukotriene synthases. PGH_2 can be converted into additional prostaglandins, including prostaglandin E2 (PGE_2), prostacyclin and thromboxanes.[70]

Our results suggest that lipid droplets in the breast epithelial cell and breast adipocytes differ not only in size, but also in biochemical composition. It indicates these lipid bodies must play different role in cancer pathology. The mechanisms leading to the differences in adipose and lipid droplet composition are unclear but are likely to be important for understanding the role of lipid droplets in cancer development.

Most of the acetyl-CoA used for *de novo* fatty acids (FA) and cholesterol biosynthesis is generated from glucose via the conversion of pyruvate to citrate in the tricarboxylic acid (TCA) cycle. However, recent evidence suggests that cancer cells are also able to generate citrate for FA biosynthesis through the reductive metabolism of glutamine.[71-73] Moreover, direct incorporation of acetate could also contribute to the pool of cytoplasmic acetyl-CoA that is used for lipid biosynthesis in cancer cells, at least under certain conditions.[74]

The results in Fig. 6 show clear indication of adipocyte differentiation. As we showed the main contribution to the differentiation originate from the triacylglycerides and fatty acids chemical composition. However, the differentiation is also associated with the surface proteins. Proteomics studies have identified hundreds lipid droplet-associated proteins.[75-77]

To learn more about the chemical composition of the lipid droplets let us focus on the proteome profile. Fig. 6 shows that the lipid droplets have the main band at 2930 cm^{-1} and additional component at 2962 cm^{-1} which is larger in MDA-MB-231 compared to MCF7 which may indicate that it increases with cancer aggressiveness. The same component is clearly visible in the difference spectra in Fig. 4. This additional component must origin from proteins.

The first lipid droplet-associated proteins identified were the perilipins and related proteins, which have important metabolic roles in the control of triacylglycerol storage and release from lipid droplets.[78,79] Perilipin is localized at the surface of lipid droplets and acts as a protective coating from the body's natural lipases, such as hormone-sensitive lipase which breaks

triglycerides into glycerol and free fatty acids for use in metabolic process of lipolysis.[78] Some of the most frequently associated proteins include enzymes involved in triacylglycerol and phospholipid biosynthesis (acyl-CoA: diacylglycerol acyltransferase 2, acyl-CoA synthetase; CTP: phosphocholine cytidylyltransferase), membrane-trafficking proteins (ARF1, Rab5, Rab18), and the adipose tissue triacylglycerol lipase (ATGL).[25,80,81]

To evaluate more formally the predictive validity and robustness of the pathway signatures emerging from the Raman analysis, PCA study was applied.

Fig. 8 shows the PCA score plot (model: smoothing, baseline, normalization, first derivative) for all the recorded Raman spectra of the breast epithelial cells. PC1, PC2, and PC3 scores accounted for 43.75%, 6.86%, 4.84% respectively of the total variance in the dataset. The PCA score plot shows good separation between the three arbitrary classes and discriminates the nonmalignant, mildly malignant and malignant metastatic human breast cancer in MCF10A, MCF7, MDA-MB-231 cell line cultures cells as shown in Fig. 8. The dominant molecular signature that discriminate between nonmalignant (MCF10A), mildly malignant (MCF7) and malignant (MDA-MB-231) cells, as well as between the various level of aggressiveness of cancer originates from lipid metabolism occurring in the lipid droplets.

Fig. 8 PCA score plot (model: smoothing, baseline, normalization, 1-st derivative) for the Raman spectra of the breast epithelial cells: MCF10A (blue circles, •), MCF7 (green triangles, ▼) MDA-MB-231 (red triangles, ▼), integration time 20 sec, 2 accumulations, laser power 38 mW, step 1.2 cm^{-1}, 2600-3940 cm^{-1}.

Interestingly, PCA analysis presented in Fig. 8 shows that the discrimination between normal and diseased cells is higher for MCF7 than for MDA-MB-231 compared to the control MCF10A. This suggests that fatty acids (FA) biosynthesis is a feature of early stages of cancer development. More-advanced tumours show reduced FA biosynthesis which is consistent with reduced proliferation but activation of an antioxidant signature of cancers.[82] This also suggests that anabolic processes are more important during the initial expansion phase of early tumours whereas the advanced disease is more dependent on processes required for the detoxification of reactive oxygen species (ROS).

The PCA analysis demonstrates that the Raman signatures of oncogenic pathways can distinguish the malignant cells expressing the oncogenic activity (MCF7 and MDA-MB-231) from the control normal cells (MCF10A). The analysis clearly distinguishes and predicts the state of an oncogenic pathway.

Conclusions

This paper examines some of the alterations in lipid metabolism that have been reported in cancer, at both cellular and tissue levels, and discuss how they contribute to different aspects of tumourigenesis. The picture that emerges from the analysis of the Raman results provide evidence that cancer cells show specific alterations in different aspects of lipid metabolism. Changes in lipid metabolism can affect numerous cellular processes, including cell growth, proliferation, and differentiation through various mechanisms including the signaling functions, availability of structural lipids for the synthesis of membranes, and energy homeostasis.

We have shown that Raman imaging provides new insights into lipid metabolism in cancers by controlling the level of the synthesis and degradation of lipids. The conventional methods (e.g. liquid chromatography - mass spectrometry (LC-MS)) cannot give spatial information about chemical composition in defined cellular compartments and must rely on bulk or fractionated analyses of extracted components. Raman spectroscopy and imaging can take advantage of high spatial resolution and intrinsic molecular differences between various chemicals in biological structures to construct free-label images that traditionally require the introduction of tags or stains.

We have found that lipid composition of cytoplasmic lipid droplets in the human breast epithelial cells and in large adipocytes of the breast tissue is different. The adipocytes in the cancerous breast tissue is dominated by triglycerides of oleic and linoleic acid. By contrast, non-adipocyte lipid droplet in the cancerous epithelial cells contains triglycerides and fatty acids dominated by arachidonic acid profile. It suggests that lipid droplet synthesis and growth is stimulated by different pathways compared to adipocytes. This important finding may indicate that the lipid droplets are potential bodies for localization of enzymes responsible for formation of eicosanoids that are produced from arachidonic acid, a polyunsaturated 20-carbon fatty acid. Our results are in agreement with numerous reports on lipid droplets abundantly present in inflammation and cancer,[28,69] which are rich in esterified arachidonate.

Our results demonstrate that the number of cytoplasmic lipid droplets in live nonmalignant MCF10A breast cells is ≈2 times lower than in a mildly malignant breast cells (MCF7) and ≈4 times lower than in a highly malignant breast cells (MDA-MB-231). Thus, an increased amount of lipid droplets correlates with increased aggressiveness of cancer. The increased amount of cytoplasmic lipid droplets in the human breast cell may be closely related to increased rate of lipid synthesis in cancerous tissues. The enhanced lipid content in malignant breast cancer cells may come from high rate synthesis of fatty acid and phospholipids. Targeting lipid metabolism that can be monitored by Raman microspectroscopy may offer novel therapeutic strategies for cancer treatment.

Acknowledgements

This work was supported by the National Science Center of Poland (grant UMO-2012/07/B/ST4/01588), Dz. St. 2014, the Foundation for Polish Science (START 2014), and Medical University of Lodz - grant 503/6-099-01/503-01.

Notes and references

[a]*Lodz University of Technology, Institute of Applied Radiation Chemistry, Laboratory of Laser Molecular Spectroscopy, Wroblewskiego 15, 93-590 Lodz, Poland*
[b]*Department of Biomedical Chemistry, Medical University of Lodz, Mazowiecka 6/8, 92-215 Lodz, Poland*
[*]*Corresponding author: Professor Halina Abramczyk; Address: Wroblewskiego 15, 93-590 Lodz, Poland; Fax: +48 42 6840043; Telephone: +48 42 6313175 and +48 42 6313188; E-mail: abramczy@mitr.p.lodz.pl*

1 H. Abramczyk and B. Brozek–Pluska, *Chem. Rev.*, 2013, **113**, 5766–5781.
2 H. Abramczyk, B. Brozek-Pluska, M. Tondusson and E. Freysz, *J. Phys. Chem. C*, 2013, **117**, 4999–5013.
3 J. Surmacki, J. Musiał, R. Kordek and H. Abramczyk, *Molecular Cancer*, 2013, **12**:48.
4 O. Warburg, *Science,* 1956, **123**, 309-314.
5 R.A. Cairns, I.S Harris and T.W. Mak, *Nature Reviews Cancer,* 2011, **11**, 85-95.
6 H. Abramczyk, B. Brozek-Pluska, J. Surmacki, J. Jablonska-Gajewicz and R. Kordek, *Progress in Biophysics and Molecular Biology,* 2012, **108**, 74-81.
7 C. Nieva, M. Marro, N. Santana-Codina, S. Rao, D. Petrov and A. Sierra, *PLOS ONE*, 2012, **7**, 1-10.
8 X. Bi, B. Rexer, C. L. Arteaga, M. Guo and A. Mahadevan-Jansen, *Journal of Biomedical Optics,* 2014, **19**, 1-6.
9 M. Hedegaard, Ch. Krafft, H. J. Ditzel, L. E. Johansen, S. Hassing and J. Popp, *Analytical Chemistry,* 2010, **82**, 2797-2802.
10 M. Hilvo, C. Denkert, L. Lehtinen, B. Müller, S. Brockmöller, T. Seppänen-Laakso, J. Budczies, E. Buche, L. Yetukuri, S. Castill, E. Berg, H. Nygren, M. Sysi-Aho, J. L. Griffin, O. Fiehn, S. Loibl, C. Richter-Ehrenstein, C. Radke, T. Hyötyläinen, O. Kallioniemi, K. Iljin and M. Oresic, *Cancer Research,* 2011, **71**, 3236-3245.
11 K. Bhalla, B. J. Hwang, R. E. Dewi, L. Ou, W. Twaddel, H. B. Fang, S. B. Vafai , F.Vazquez, P. Puigserver, L. Boros and G. D. Girnun, *Cancer Research,* 2011, **71**, 6888-6898.
12 R. Munir, H. Usman, S. Hasnain, K. Smans, H. Kalbacher and N. Zaidi, *Biochimie*, 2014, **102**, 9-18.
13 F. Baenke, B. Peck, H. Miess and A. Schulze, *Disease Models and Mechanisms,* 2013, **6**, 1353-1363.
14 E. Rysman, K. Brusselmans, K. Scheys, L. Timmermans, R. Derua, S. Munck, P.P. Van Veldhoven, D. Waltregny, V. W. Daniels, J. Machiels, F. Vanderhoydonc, K. Smans, E. Waelkens, G. Verhoeven and J. V. Swinnen, *Cancer Research*, 2010, **70**, 8117–8126.
15 B. Griffiths, C. A. Lewis, K. Bensaad, S. Ros, Q. Zhang, E. C. Ferber, S. Konisti, B. Peck, H. Miess, P. East, M. Wakelam, A. L. Harris and A. Schulze, *Cancer & Metabolism*, 2013, **1**, 1-21.
16 A. Mahadevan –Jansen and R. R. Richards-Kortum, *Journal of Biomedical Optics*, 1996, **1**, 31-70.
17 N. J. Kline and P. J. Treado, *Journal of Raman Spectroscopy*, 1997, **28**, 119-124.
18 M. Diem, M. Miljkovic, B. Bird, T. Chernenko, J. Schubert, E. Marcsisin, A. Mazur, E. Kingston, E. Zuser, K. Papamarkakis and N. Laver, *Spectroscopy: An International Journal,* 2012, **27**, 463-496.
19 A. Mahadevan-Jansen, M. F. Mitchell, N. Ramanujamf, A. Malpica, S. Thomsen, U. Utzinger and R. Richards-Kortumt, *Photochemistry and Photobiology,* 1998, **68**, 123-132.
20 M. Beller, K. Thiel, P. J. Thul and H. Jäckle, *FEBS Letters*, 2010, **584**, 2176–2182.
21 S. D. Kohlwein, M. Veenhuis and I. J. Van der Klei, *Genetics*, 2013, **193**, 1-50.
22 D. J. Murphy, *Progress in Lipid Research*, 2001, **40**, 325–438.
23 K. Reue and E. Board, *Journal of Lipid Research*, 2011, **52**, 1865-1868.
24 A. R. Thiam, R. V. Farese Jr and T. C. Walther, *Nature Reviews Molecular Cell Biology*, 2013, **14**, 775-786.
25 Y. Guo, T. C. Walther, M. Rao, N. Stuurman, G. Goshima, K. Terayama, J. S. Wong, R. D. Vale, P. Walter and R. V. Farese, *Nature*, 2008, **453**, 657–661.
26 H. Zirath, A. Frenzel, G. Oliynyk, L. Segerström, U. K. Westermark, K. Larsson, M. Munksgaard Persson, K. Hultenby, J. Lehtiö, Ch. Einvik, S. Påhlman, P. Kogner, P. J. Jakobssonb and M. A. Henriksson, *PNAS*, 2013, **110**, 10258-10263.
27 C. R. Santos and A. Schulze, *FEBS Journal*, 2012, **279(15)**, 2610-2623.
28 P. T. Bozza and J. P. B. Viola, *Prostaglandins, Leukotrienes and Essential Fatty Acids*, 2010, **82**, 243-250.
29 K. L. Erickson and N. E. Hubbard, *Prostaglandins, Leukotrienes and Essential Fatty Acid*, 2010, **82**, 237-241.
30 R. Chowdhury, B. Jana, A. Saha, S. Ghosh and K. Bhattacharyya, *Med. Chem. Commun*. 2014, **5**, 536-539.
31 E. J. Delikatny, W. A. Cooper, S. Brammah, N. Sathasivam and D. C. Rideout, *Cancer Research*, 2002, **62**, 1394-1400.
32 K. Glunde, V. Raman, N. Mori and Z. M. Bhujwalla, *Cancer Research*, 2005, **65**, 11034-11043.
33 P. N. Munster, M. Srethapakdi, M. M. Moasser and N. Rosen, *Cancer Research,* 2001, **61**, 2945-2952.
34 I. Barba, M. E. Cabanas and C. Arus, *Cancer Research*, 1999, **59**, 1861-1868.
35 L. L. Moyec, R. Tatoud , M. Eugene, C. Gauville, I. Primot, D. Charlemagne and F. Calvo, British Journal of *Cancer*, 1992, **66**, 623-628.
36 J. White, *J Natl Cancer Inst*, 2000, **92**, 443.
37 M. Suzuki, Y. Shinohara, Y. Ohsaki and T. Fujimoto, *Journal of Medical Microscopy*, 2011, **60**, 101-116.
38 H. Abramczyk, B. Brozek-Pluska, J. Surmacki, J. Jablonska and R. Kordek, *Journal of Molecular Liquids*, 2011, **164**, 123-131.
39 B. Brozek-Pluska, J. Musial, R. Kordek, E. Bailo, T. Dieing and H. Abramczyk, *Analyst,* 2012, **137**, 3773-3780.
40 L.L. Listenberger, X. Han, S. E. Lewis, S. Cases, R. V. Farese, D. S. Ory and J. E. Schaffer, *Proceedings of the National Academy of Sciences of the United States of America,* 2003, **100**, 3077-3082.
41 X. Nan, J-X. Cheng and X. S. Xie, *Journal of Lipid Research*, 2003, **44**, 2202-2208.
42 T. T. Le, S. Yue, J-X. Cheng, *Journal of Lipid Research*, 2010, **51**, 3091-102.
43 C. L. Evans and X. S. Xie, *Annual Review of Analytical Chemistry*, 2008, **1**, 883-909.
44 R. Mitra, O. Chao, Y. Urasaki, O. B. Goodman and T. T. Le, *BMC Cancer,* 2012, **12**, 1-9.

45 L. Bednarova, J. Palacky, V. Bauerova, O. Hruskova-Heidingsfeldova, I. Pichova and P. Mojzes, *Spectroscopy: An International Journal*, 2012, **27**, 503-507.

46 C. A. Schütz, D. Staedler, K. Crosbie-Staunton, D. Movia, C. Ch. Bernasconi, B. H. Kenzaoui, A. Prina-Mello, and L. Juillerat-Jeanneret, *Int. J. Nanomedicine*, 2014, **9**, 3481-3498.

47 C. J. Behrend, C. P. Tarnowski and M. D. Morris, *Applied Spectroscopy*, 2002, **56**, 1458-1461.

48 U. B. Cappel, I. M. Bell and L. K. Pickard, *Applied Spectroscopy*, 2010, **64**, 195-200.

49 A. Savitzky and M. J. E. Golay, *Analytical Chemistry*, 1964, **36**, 1627-1639.

50 B. M. Wise, N. B. Gallagher, R. Bro, J. M. Shaver, W. Windig and R. S. Koch. PLS_Toolbox Version 4.0 for use with MATLAB™, Eigenvector Research, Inc.3905 West Eaglerock Drive, Wenatchee, WA 98801.

51 B. Brozek-Pluska, J. Jablonska-Gajewicz, R. Kordek and H. Abramczyk, *J. Med. Chem.*, 2011, **54**, 3386-3392.

52 P. Bostrom, M. Rutberg, J. Ericsson, P. Holmdahl, L. Andersson, M. A. Frohman, J. Boren and S. O. Olofsson, *Arterioscler Thromb Vasc Biol.*, 2005, **25**, 1945-1951.

53 J. Surmacki, B. Brozek-Pluska, R. Kordek and H. Abramczyk, *Analyst*, 2015, DOI: 10.1039/C4AN01876A.

54 A. Nijssen, T.C. Bakker Shut, F. Heule, P. J. Caspers, D. P. Hayes, M. H. Neumann and G. J. Puppels, *J. Invest Dermatol*, 2002, **119**, 64-69.

55 A. Hemelink, A. Brauer, P. Lasch and D. Naumann, *Analyst*, 2009, **134**, 1149-1153.

56 Q. Wu, W. H. Nelson, S. Elliot, J. F. Sperry, M. Feld, R. Dasari and R. Manoharan, *Analitycal Chemisty*, 2000, **72**, 2981-2986.

57 K. A. Hartman, N. Clayton and G. J. Thomas, *Biochemical and Biophysical Rearch Communications*, 1973, **50**, 942-949.

58 A. Mahadevan-Jansen and R. Richards-Kortum, *Journal of Biomedical Optics*, 1996, **1**, 31-70.

59 A. C. S. Talari, C. Yorucu, C. A. Evans, I. Holen, S. Rehman, R. E. Coleman and I. U. Rehman, Spectroscopy of Cancer: Raman Spectroscopic Analysis of Different Subtypes of Breast Cancer Tissues and Cell Lines, 2013, 12-13.

60 J. De Gelder, K. De Gussem, P. Vandenabeele and L. Moens, *Journal of Raman Spectroscopy*, 2007, **38**, 1133–1147.

61 Z. Huang, A. McWilliams, H. Lui, D. I. McLean, S. Lam and H. Zeng, *International Journal of Cancer*, 2003, **107**,1047-1052.

62 S. Leikin, V. A. Parsegian, W-H Yang and G. E. Walrafen, *Proceedings of the National Academy of Sciences of the United States of America,* 1997, **94**, 11312-11317.

63 L. Silveira, F. L. Silveira, B. Bodanese ,R. A. Zângaro and M. T. T. Pacheco, *J. Biomed. Opt.*, 2012, **17**, 1-11.

64 J. A. Menendez and R. Lupu, *Nature Reviews Cancer*, 2007, **7**, 763-777.

65 G. Medes, A. Thomas and S. Weinhouse, *Cancer Research*, 1953, **13**, 27-29.

66 A. Vazquez-Martin, R. Colomer, J. Brunet, L. Lupu and J. A. Menendez, *Cell Proliferation*, 2008, **41**, 59-85.

67 J. A. Menendez, L. Vellon, I. Mehmi, B. P. Oza, S. Roperto, R. Colomer and R. Lupu, *Proceedings of the National Academy of Sciences of the United States of America*, 2004, **101**, 10715-10720.

68 A. L. Albright and J. S. Stern, Adipose tissue. In: Encyclopedia of Sports Medicine and Science, Fahey TD (Editor). Internet Society for Sport Science: http://sportsci.org. 30 May 1998.

69 A. J. Quayle, E. M. Porter, A. A. Nussbaum, Y. M. Wang, C. Brabec, K. P. Yip and S. C. Mok, *J Pathol*, 1998, **152**, 1247-1258.

70 M. P. Wymann and R. Schneiter, *Nature Reviews Molecular Cell Biology*, 2008, **9**, 162–176.

71 Ch. M. Metallo, P. A. Gameiro, E. L. Bell, K. R. Mattaini, J. Yang, K. Hiller, Ch. M. Jewell, Z. R. Johnson, D. J. Irvine, L. Guarente, J. K. Kelleher, M. G. Vander Heiden, O. Iliopoulos and G. Stephanopoulos, *Nature*, 2012, **481**, 380–384.

72 A. R. Mullen, W. W. Wheaton, E. S. Jin, P-H. Chen, L. B. Sullivan, T. Cheng, Y. Yang, W. M. Linehan, N. S. Chandel and R. J. DeBerardinis, *Nature*, 2012, **481**, 385–388.

73 D. R. Wise, P.S. Ward, J. E. S. Shay, J. R. Cross, J. J. Gruber, U. M. Sachdeva, J. M. Platt, R. G. DeMatteo, M. C. Simon and C. B. Thompson, *Proc Natl Acad Sci USA*, 2011, **108**, 19611-19616.

74 N. Zaidi, J. V. Swinnen and K. Smans, *Cancer Research*, 2012, **72**, 3709–3714.

75 R. Bartz, J. K. Zehmer, M. Zhu, Y. Chen, G. Serrero, Y. Zhao, P. Liu, *Journal of Proteome Research*, 2007, **6**, 3256-3265.

76 M. Beller, D. Riedel, L. Jansch, G. Dieterich, J. Wehland, H. Jackle, R. P. Kuhnlein, *Mol Cell Proteomics*, 2006, **5**, 1082 – 1094.

77 C. C. Wu, K. E. Howell, M. C. Neville, J. R. Yates III, J. L. McManaman, *Electrophoresis*, 2000, **21**, 3470-3482.

78 D. L. Brasaemle, V. Subramanian, A. Garcia, A. Marcinkiewicz and A. Rothenberg, *Mol Cell Biochem*, 2009, **326**, 15-21.

79 A. S. Greenberg, J. J. Egan, S. A. Wek, N. B. Garty, E. J. Blanchette-Mackie and C. Londos, *Journal of Biological Chemistry*, 1991, **266**, 11341-11346.

80 L. Kuerschner, Ch. Moessinger and C. Thiele, *Traffic*, 2008, **9**, 338-352.

81 S. J. Stone, M. C. Levin, P. Zhou, J. Han, T. C. Walther and R. V. Farese Jr, *The Journal of Biological Chemistry*, 2009, **284**, 5352-5361.

82 L. Jerby, L. Wolf, C. Denkert, G. Y. Stein, M. Hilvo, M. Oresic, T. Geiger and E. Ruppin, *Cancer Research*, 2012, **72**, 5712-5720.

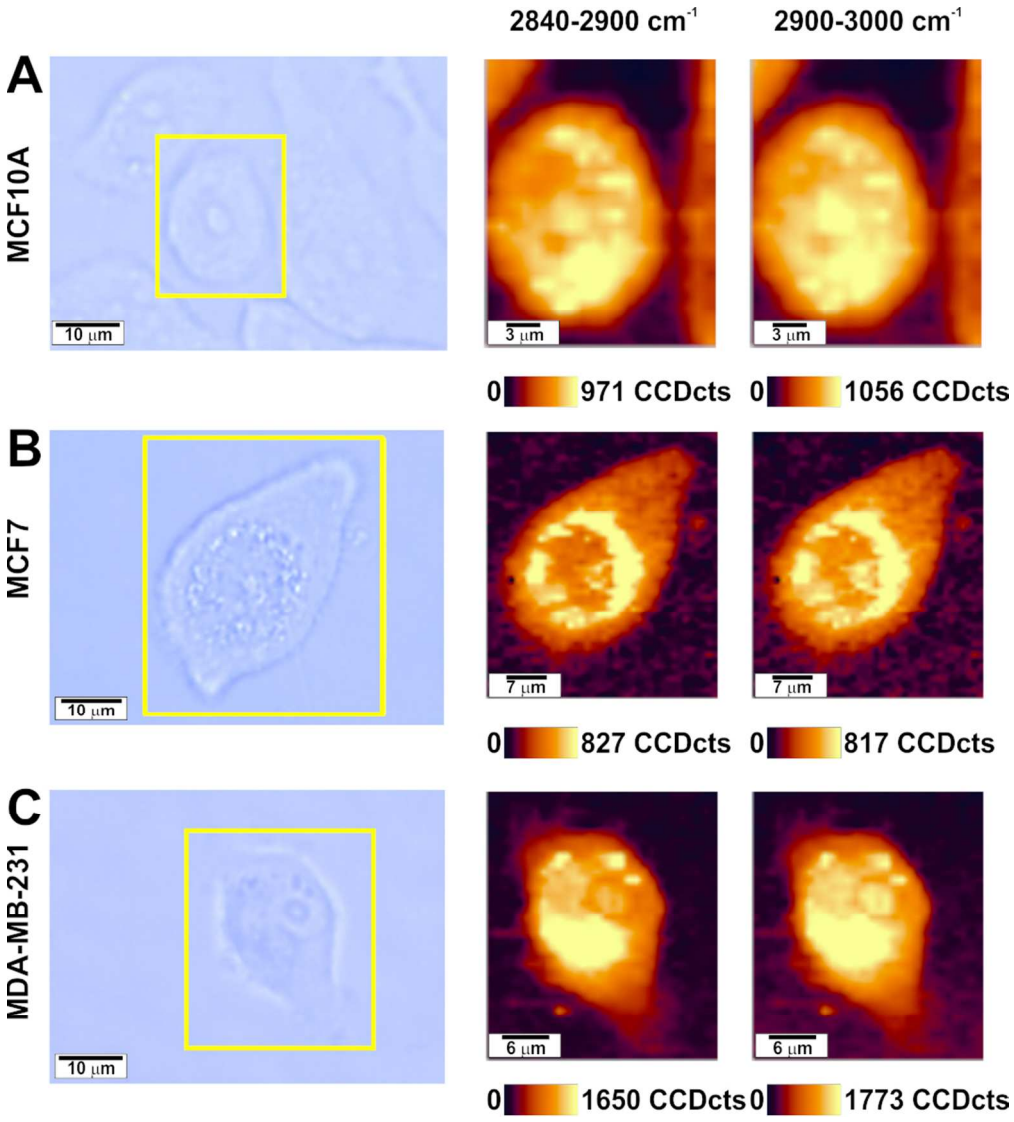

The video images and respective Raman images of MCF10A (A), MCF7 (B) and MDA-MB-231 (C) intracellular structures: lipid structure (triacylglycerides (TAGs), fatty acids (FA) and cholesterol esters (CEs) (2840-2900 cm^{-1}), lipid-protein structures (2900-3000 cm^{-1}) of live breast cells in PBS.
90x99mm (300 x 300 DPI)

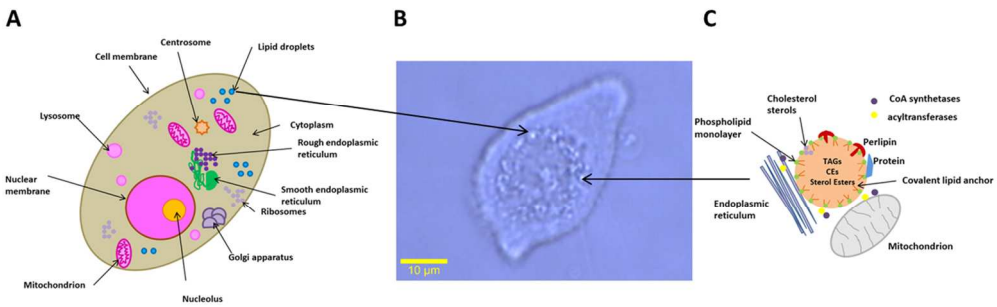

Cross section of an animal cell (A), video image of a single cell of MCF7 (B) and lipid droplet (C).
252x77mm (142 x 142 DPI)

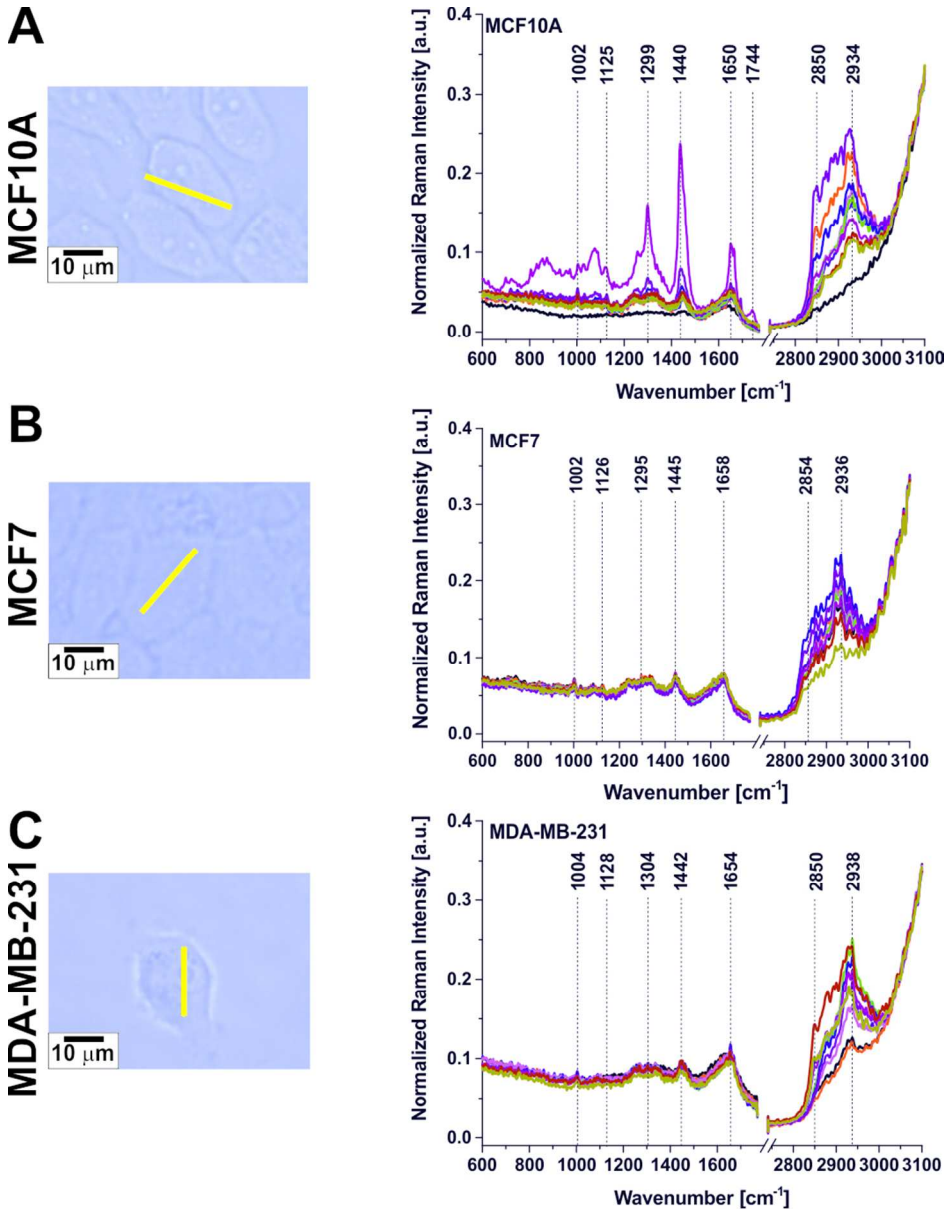

Raman spectra across the marked lines inside the cells: MCF10A (A), MCF7 (B) and MDA-MB-231 (C). Spectra were normalized to the integral intensity of the water OH-stretching band at 3400 cm^{-1} as an intensity standard.
90x115mm (300 x 300 DPI)

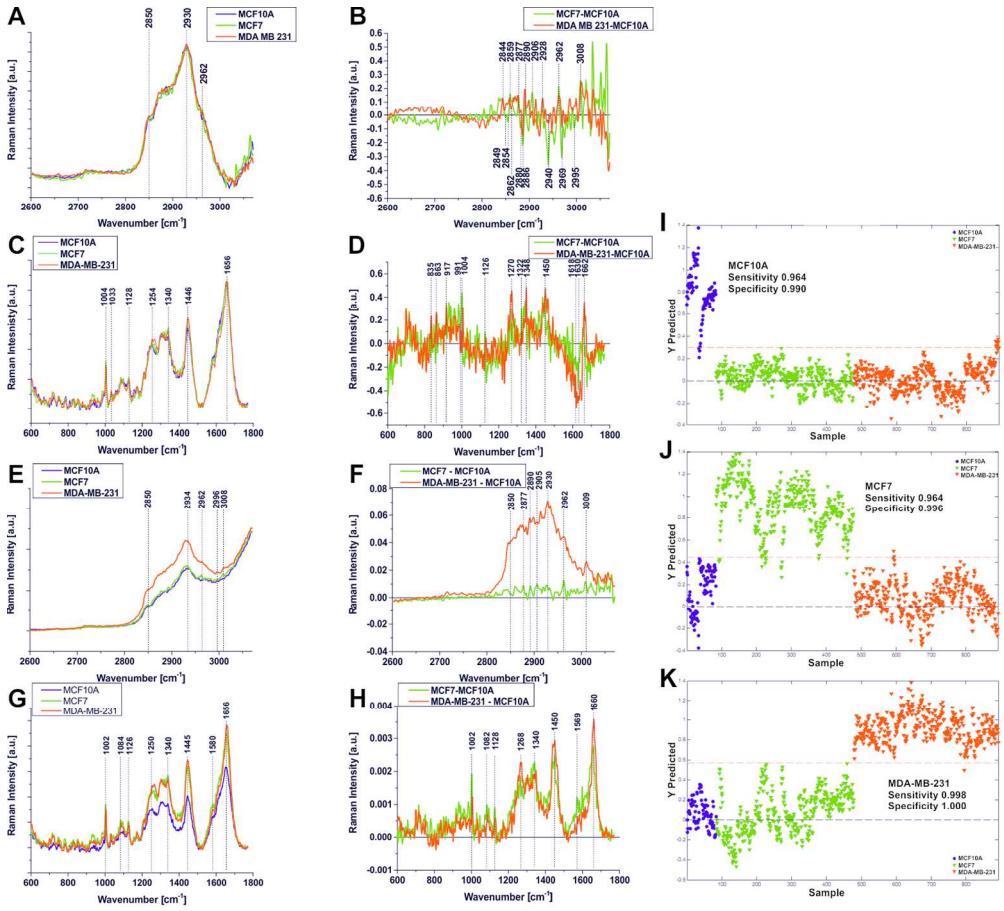

Average Raman spectra (A,C,E,G) and average difference Raman spectra (B,D,F,H); (A-D) model preprocessing: smoothing, baseline, Standard Normal Variate (SNV); (E-H) model preprocessing: smoothing, baseline, spectra are normalized to the integral intensity of the water OH-stretching band at 3400 cm^{-1} as an intensity standard; Cross-validated PLSDA Y-prediction plots for MCF10A (I), MCF7 (J), MDA-MB-231 (K).
140x125mm (300 x 300 DPI)

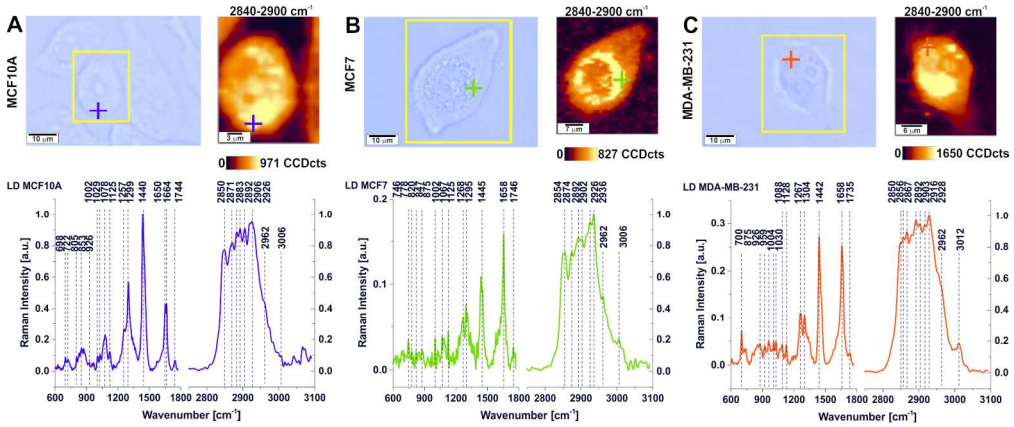

Video images, label-free Raman images (2840-2900 cm^{-1}) and Raman spectra from the characteristic structures (marked by the cross) of the lipid droplets in the live cells MCF10A (A), MCF7 (B) and MDA-MB-231 (C).
189x79mm (300 x 300 DPI)

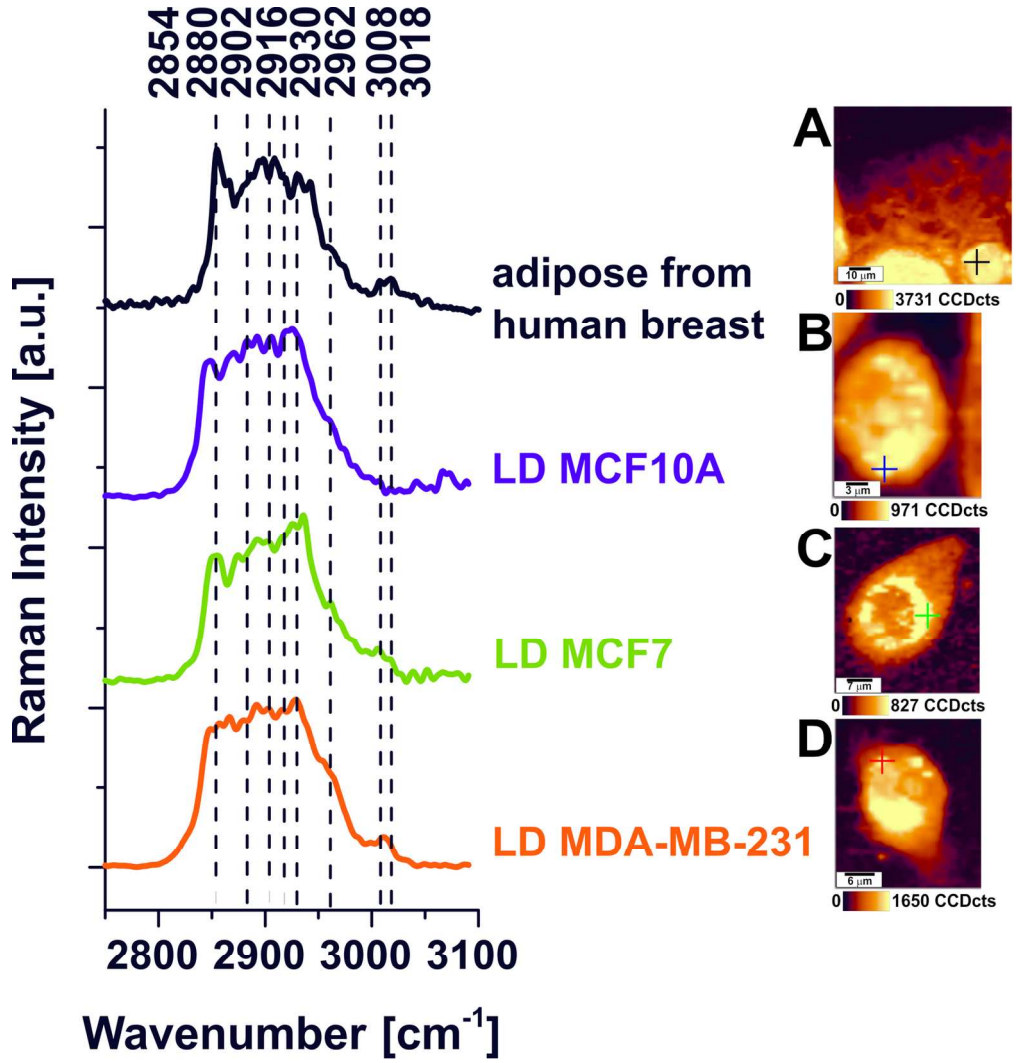

Comparison of the Raman spectra from the human adipose tissue (at the point marked with the green cross +) in the cancerous breast tissue (infiltrating ductal carcinoma, P104) and from the lipid droplets in the epithelial cells of MCF10A, MCF7 and MDA-MB-231.
146x154mm (300 x 300 DPI)

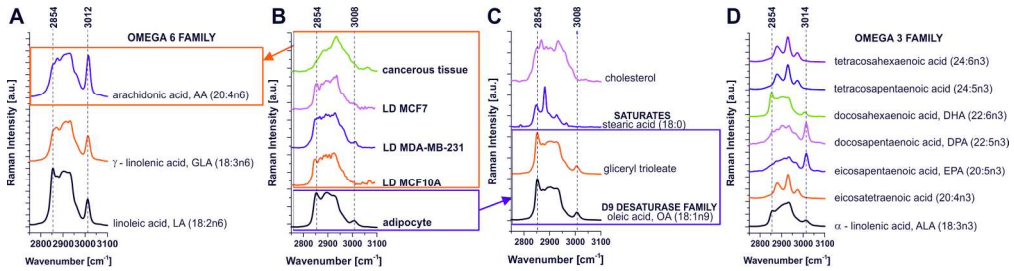

Comparison of Raman spectra of adipocyte from the cancerous breast tissue (infiltrating ductal carcinoma) of patient 104 (adipocyte), lipid droplets from the nonmalignant and malignant epithelial cells: MCF10A, MCF7, MDA-MB-231 (B) with selected omega 6 family fatty acids: linoleic acid (LA), α-linolenic acid (GLA), arachidonic acid (AA) (A); oleic acid (OA), gliceryl trioleate, stearic acid, cholesterol (C), and selected omega 3 fatty acids: γ-linolenic acid (ALA), eicosatetraenoic acid, eicosapentaenoic acid (EPA), docosapentaenoic acid (DPA), docosahexaenoic acid (DHA), tetracosapentaenoic acid, tetracosahexaenoic acid (D).
189x49mm (300 x 300 DPI)

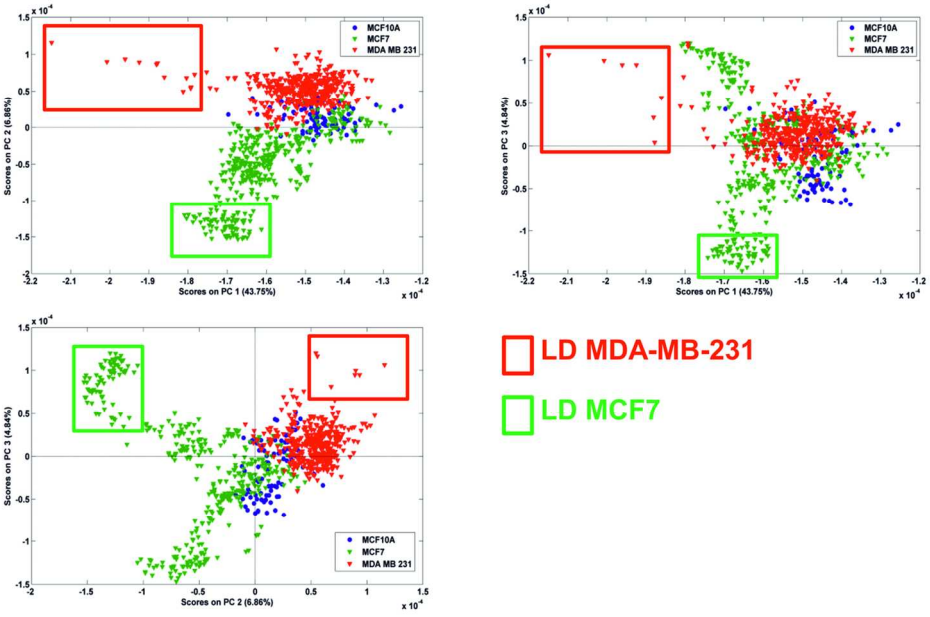

PCA score plot (model: smoothing, baseline, normalization, 1-st derivative) for the Raman spectra of the breast epithelial cells: MCF10A (blue circles, •), MCF7 (green triangles, ▼) MDA-MB-231 (red triangles,▼), integration time 20 sec, 2 accumulations, laser power 38 mW, step 1.2 cm^{-1}, 2600-3940 cm^{-1}.
125x78mm (300 x 300 DPI)

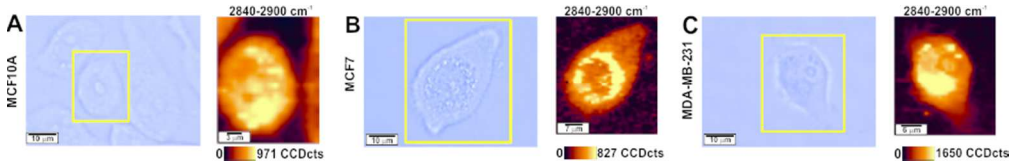

We analyzed the composition of lipid droplets in nonmalignant and malignant human breast epithelial cell lines and discuss the potential of lipid droplets as a prognostic marker in breast cancer.
80x12mm (300 x 300 DPI)